PNAS RESEARCH ARTICLE | CHEMISTRY
BIOPHYSICS AND COMPUTATIONAL BIOLOGY

Origins of synergy in multilipid lubrication

Yifeng Cao[a,1,2,3,4], Di Jin[a,3,4], Nir Kampf[a], and Jacob Klein[a,4]

Affiliations are included on p. 9.

Edited by Noel Clark, University of Colorado Boulder, Boulder, CO; received April 25, 2024; accepted October 3, 2024

Lipid bilayers, ubiquitous in living systems, form lubricious boundary layers in aqueous media, with broad relevance for biolubrication, especially in mechanically stressed environments such as articular cartilage in joints, as well as for modifying material interfacial properties. Model studies have revealed efficient lubricity by single-component lipid bilayers; synovial joints, however (e.g. hips and knees), comprise over a hundred different lipids, raising the question of whether this is natural redundancy or whether it confers any lubrication benefits. Here, we examine lubrication by progressively more complex mixtures of lipids representative of those in joints, using a surface forces balance at physiologically relevant salt concentrations and pressures. We find that different combinations of such lipids differ very significantly in the robustness of the bilayers to hemifusion under physiological loads (when lubrication breaks down), indicating a clear lubrication synergy afforded by multiple lipid types in the bilayers. Insight into the origins of this synergy is provided by detailed molecular dynamics simulations of potential profiles for the formation of stalks, the essential precursors of hemifusion, between bilayers of the different lipid mixtures used in the experiments. These reveal how bilayer hemifusion—and thus lubrication breakdown—depends on the detailed lipid bilayer composition, through the corresponding separation into domains that are better able to resist stalk formation. Our results shed light on the role of lipid-type proliferation in biolubrication synergy, point to improved treatment modalities for common joint diseases such as osteoarthritis, and indicate how lipid-based interfacial modification in a materials context may be optimized.

lipid bilayers | biolubrication | lipid mixtures | molecular dynamics | surface forces

Significance

Hundreds of millions worldwide suffer from osteoarthritis (OA), a debilitating disease due to degradation of the articular cartilage coating our joints and associated with its lubrication breakdown. This lubrication has been attributed to lipids at the cartilage surface, but while model studies on single-component lipids show strong friction reduction, joints contain over a hundred different lipids, and the additional lubrication benefits, if any, of such lipid multiplicity are not understood. Studying lubrication by different lipid mixtures, we find that certain mixtures are greatly superior to others, demonstrating clear lubrication synergy. By performing detailed simulations, we are able to clarify the molecular origins of this. Our findings elucidate nature's biolubrication strategies and may point to better lipid-based intra-articular treatments for OA.

Lipids are ubiquitous in living systems, where they play a wide variety of roles, including energy storage, signaling, and acting as structural components of cell membranes (1). Our interest is in their role in modifying interfacial properties, particularly frictional energy dissipation, both in living systems and in a materials context, as for example, on articular cartilage in synovial joints (2) or on lipid-incorporating hydrogel surfaces (3).

Synovial joints (such as hips and knees) have evolved as highly efficient lubrication systems, where the friction at the cartilage surfaces, which are compressed and slide past each other as joints articulate, is associated with friction coefficients μ (=[force to slide]/[load]) as low or lower than 0.001 (4). Such low friction is crucial for their well-being (4, 5), in particular for suppressing wear-related cartilage degradation (6), a leading symptom of osteoarthritis (OA), the most widespread joint pathology. Cartilage lubricity has been attributed both to the role of interstitial fluid pressure within the tissue and largely to strongly lubricating boundary layers at its surface, whose molecular origins have been extensively studied (4, 7–10). In recent years, surface-attached phospholipid (PL) layers, in particular phosphatidylcholines (PCs), which are ubiquitous in joints, have been shown, as noted above, to act as exceptionally good boundary lubricants at both synthetic and at biological surfaces (5, 11–14) (recalling that boundary lubrication is largely independent of the underlying substrate). Model studies have shown that bilayers of zwitterionic PCs (11, 14) and sphingomyelin (SM) lipids (15) result in low friction up to physiological pressures, with μ down to 10^{-4} or lower, comparable to that of articular cartilage in joints. This arises through the hydration lubrication mechanism (16) active at the highly hydrated phosphocholine groups exposed by the surface-attached lipid bilayers (17, 18) at the slip-plane, and it has been proposed that similar boundary layers are present at the articular cartilage surface, providing its excellent lubricity (2, 4, 5, 7). To date, studies of boundary lubrication by lipids have all, with few exceptions (19–21), examined single-component PCs (8, 11, 14, 17, 22, 23); healthy joints, however, are known to include over a hundred different lipids, belonging to several different classes, and comprising additionally differing tail saturation levels and lengths (24–27). A key question, therefore, is whether—separately from any other functions—this proliferation of different lipids in joints holds benefits for

Author contributions: Y.C., D.J., and J.K. designed research; Y.C., D.J., and N.K. performed research; Y.C., D.J., and N.K. contributed new reagents/analytic tools; Y.C., D.J., N.K., and J.K. analyzed data; and Y.C., D.J., N.K., and J.K. wrote the paper.

The authors declare no competing interest.

This article is a PNAS Direct Submission.

[1]Present address: Institute of Zhejiang University-Quzhou, Quzhou 324000, China.

[2]Present address: College of Chemical and Biological Engineering, Zhejiang University, Hangzhou 310027, China.

[3]Y.C. and D.J. contributed equally to this work.

[4]To whom correspondence may be addressed. Email: caoyf@zju.edu.cn, di.jin@weizmann.ac.il, or jacob.klein@weizmann.ac.il.

This article contains supporting information online at https://www.pnas.org/lookup/suppl/doi:10.1073/pnas.2408223121/-/DCSupplemental.

Published November 12, 2024.

boundary lubrication at the articular cartilage surface, relative to the single-component PC layers which have been studied to date.

The major PL groups identified in synovial joints, present in the form of multilamellar and vesicular structure (28, 29), include electroneutral PC, SM, and phosphatidylethanolamine (PE), as well as, as minor components, negatively charged PLs (24, 26). The majority have at least one unsaturated tail (26), while the species and concentration of PLs in synovial joints are also affected by joint diseases, such as OA and rheumatoid arthritis (30, 31). In a previous study, we examined the interactions between membranes of a binary mixture of two PC lipids: 1,2-dipalmitoyl-*sn*-glycero-3-phosphocholine (DPPC) and 1-palmitoyl-2-oleoyl-glycero-3-phosphocholine (POPC) (21). The hemifusion of opposing bilayers composed of that DPPC/POPC mixture, and the consequent elimination of the hydration-lubricated slip-plane at the headgroup–headgroup interface, caused an abrupt increase in the friction force; the hemifusion in that case was attributed to phase separation of gel-phase and liquid phase domains.

The present study focuses on the forces acting between surface boundary layers of lipid mixtures, including the major PL classes found in healthy synovial fluid (SF) and on cartilage surfaces, to provide more general insight into the lubrication efficiency and possible synergy of multicomponent lipid boundary layers. By synergy here is meant that the effect of combining different lipids leads to better lubrication than just the sum of the parts. In particular, while it is clearly not possible to test all possible combinations of the order of 100 or more different PLs in joints (24, 26, 27), a demonstration of improved lubrication arising from particular combinations of different lipids in the boundary layers may provide insight from a biolubrication perspective as to why there is such proliferation of different lipids in joints. Extending our previous work on single-component PLs and binary PC mixtures, we take a first step to mimic the diversity of PLs in joints by adsorbing increasingly complex lipid mixtures (Table 1 and *SI Appendix*, Fig. S1 and Table S1) on a model substrate and measuring normal and frictional forces between them at physiological salt concentrations. Forces are measured using the surface force balance (SFB), where the model substrate is atomically smooth mica (negatively charged in aqueous media). Detailed molecular dynamics (MD) simulations are then used to shed strong light on the origins of the different lubrication behavior corresponding to the different lipid combinations.

Results

The three PL mixtures composed of 2, 5, and 8 lipids, designated L2, L5, and L8, respectively (Table 1), were selected to include progressively more of the major lipid classes in synovial joints (*SI Appendix*, Fig. S1 and Table S1). To approximately mimic the PLs in synovial joints, all the representative mixtures contain lipids with phosphocholine and phosphoethanolamine headgroups, which are the main lipid groups detected in the joints (as summarized in *SI Appendix*, Fig. S2), and all have unsaturated PLs as majority components. L8 included, in addition to main PL types, also cholesterol (CHOL) which is ubiquitous in physiological lipid bilayers and in SF.

Surface Morphologies. To obtain additional insight into the effect of combining the different lipids, all measurements were carried out both in the absence and in the presence of calcium ions (as the $Ca(NO_3)_2$ salt) at concentrations (2 mM) similar to their physiological concentrations that have been reported in healthy SF (32) [we note that reported Ca^{2+} concentrations in OA SF tend to be higher (32, 33)]. Size distribution and zeta potentials of small unilamellar vesicles (SUVs) of the three mixtures were characterized by dynamic light scattering (DLS) and are shown in Table 1, with all three having rather small negative potentials. We point out that addition of 2 mM Ca $(NO_3)_2$ had little effect on the DLS-measured vesicle diameters (which remained at ca. 65 nm) for L2 and L5, indicating little aggregation by the divalent ions. In contrast, L8, which included the negatively charged DPPA (at low concentration—ca. 1.4 mol%) and had a slightly more negative zeta potential, was clearly aggregated by the calcium ions, which presumably acted as adhesive linkers between the 1,2-palmitoyl-phosphatidic acid (DPPA) headgroups on the vesicles. Formation of surface assemblies of the lipids on the mica substrate was achieved by spontaneous adsorption of the vesicles from the respective dispersions (see AFM section, *Materials and Methods*), likely driven by the dipole–charge interactions of the majority-components PC-headgroup zwitterions with the mica, following which they ruptured to form bilayers on the mica. Morphologies of these bilayers were characterized by atomic force microscopy (AFM) (Fig. 1).

Surface Interactions. Normal and shear forces between the bilayer-bearing mica surfaces at different surface separations D across the respective SUV dispersions with and without added $Ca(NO_3)_2$ were directly measured using an SFB (Fig. 2*A*). Fig. 2 shows typical shear trace profiles for all three mixtures, while Fig. 3 shows their normal and friction force profiles. As seen in Figs. 2 and 3, all three mixtures showed broadly similar behavior both in their normal and in frictional interactions, as follows. The normal interactions $F_n(D)/R$ revealed a short-ranged interaction, as expected at the high salt concentration (150 mM $NaNO_3$) of the dispersions, where the Debye screening length for electrostatic interactions is less than 1 nm. Monotonic repulsions in these profiles commenced at somewhat longer range (ca. 20 to 30 nm for L2, L5 and ca. 50 nm for L8) and may be attributed to steric interactions between loosely adsorbed liposomes on the surface-attached bilayers. At higher loads—emphasized in the insets to Fig. 3*A*, *C* and *E*—the interactions showed "hard-wall" repulsions at $D \approx 10 \pm 1$ nm, indicating a bilayer on each surface. As the loads were increased, hemifusion occurred as revealed by a jump-in of the surfaces at a critical normal load, to D values indicating a single bilayer between the surfaces. On adding the calcium salt (to 2 mM Ca^{++} concentration, similar to physiological values), the normal force profiles remained essentially unchanged, save

Table 1. Compositions, averaged size, polydispersity (PdI), and zeta potential values of mixed-lipid-SUVs prepared in 150 mM $NaNO_3$ before and after adding $Ca(NO_3)_2$

Lipid composition	Dispersant	Size/nm	PdI	Zeta potential/mV
L2: POPC-POPE (in ratio 4:1)	150 mM $NaNO_3$	68.2 ± 1.2	0.064	−4.8 ± 1.6
	+2 mM $Ca(NO_3)_2$	69.6 ± 2.0	0.082	−2.3 ± 1.7
L5: DPPC-POPC-DOPC-POPE-Egg SM (1:1:1:1:1)	150 mM $NaNO_3$	65.1 ± 0.7	0.072	−1.6 ± 0.6
	+2 mM $Ca(NO_3)_2$	64.1 ± 1.1	0.066	−0.4 ± 0.2
L8: DPPC-POPC-DOPC-POPE-Egg SM-DPPA-LPC-CHOL (1:1:1:1:1:0.1:1:1)	150 mM $NaNO_3$	63.4 ± 0.7	0.057	−7.3 ± 0.3
	+2 mM $Ca(NO_3)_2$	Multiple peaks	0.440	−5.3 ± 0.3

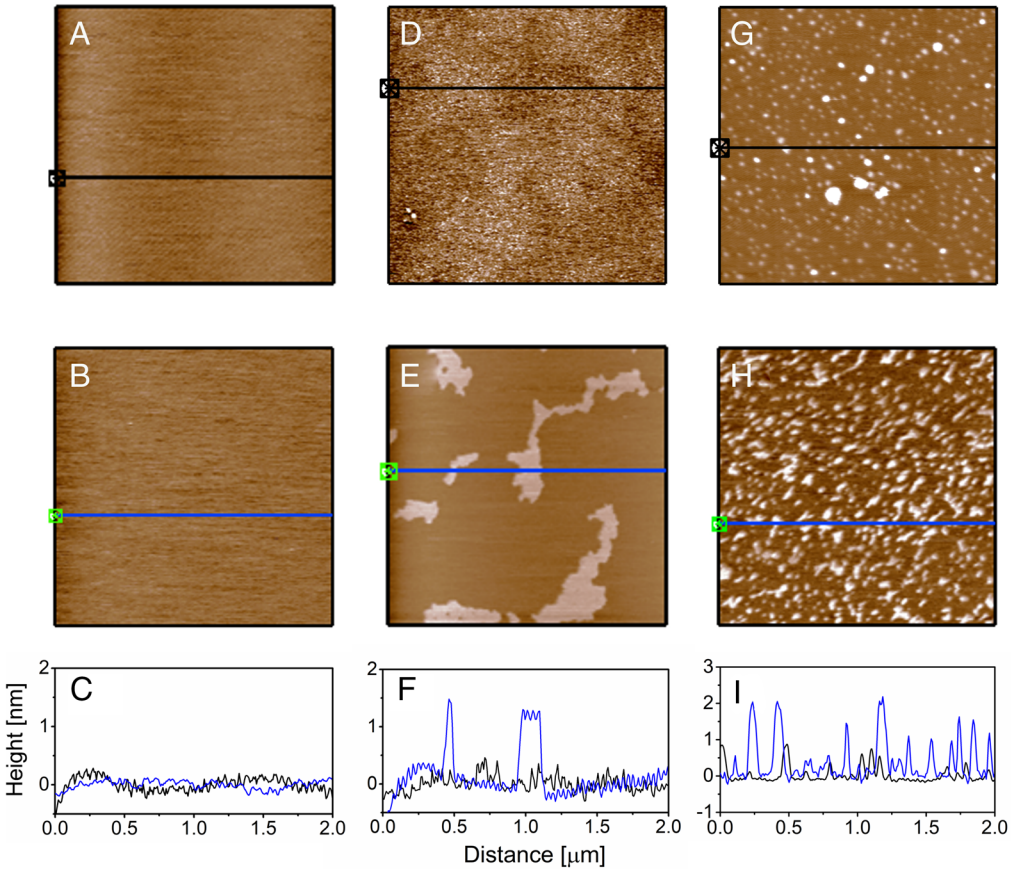

Fig. 1. AFM height images of SUVs adsorbed on mica before (*A*, *D*, and *G*) and after (*B*, *E*, and *H*) adding 2 mM Ca $(NO_3)_2$ for the L2 (*A*–*C*), L5 (*D*–*F*), and L8 (*G*–*I*) systems, respectively. All scans were performed across 0.3 mM SUV dispersion prepared in 150 mM $NaNO_3$. The size of each image is 2 μm × 2 μm. Panels (*C*), (*F*), and (*I*) in the last row are corresponding height profiles, wherein the black and blue lines represent those before and after adding 2 mM Ca $(NO_3)_2$. The phase-separated (lighter) regions in panel (*E*) are likely of the gel-phase (saturated) lipid components, DPPC and Egg SM, and occupy ca. 13% of the area scanned as analyzed by image segmentation.

that the critical load required for hemifusion greatly increased. On separation of the surfaces and reapproach, the behavior was reproducible, indicating healing of any change in the surface morphology due to the hemifusion.

The frictional interactions were also broadly similar for all three mixtures, as seen in Figs. 2 and 3*B*, *D* and *F*: At lower loads, all three mixtures had very low friction coefficients μ, down to $\mu \approx 10^{-4}$ or lower; when hemifusion occurred as the critical loads were reached, the friction force (and friction coefficient) increased abruptly, as expected. Once Ca^{++} was added, and critical loads for hemifusion became much larger (as detailed below), the friction force upon hemifusion exceeded the maximal applied shear force in the SFB and the surfaces remained in rigid contact when sheared (solid red arrows in Fig. 3*B*, *D* and *F*. In addition to these features of the interaction common to all three mixtures, below we describe additional features specific to each mixture.

L2 mixture: POPC-POPE (molar ratio 4:1), Fig. 3A and ***B.*** In Fig. 3*A*, as $F_n(D)$ increases, *D* decreases gradually until at a critical normal load, it shifts abruptly from 9.8 ± 0.5 to 5.1 ± 1.0 nm, indicating that two PL bilayers hemifuse into one (*Inset* to Fig. 3*A*). On further loading, the trapped bilayer is squeezed out of the contact area, as *D* decreases from 4.1 ± 0.9 nm to 0.2 ± 0.4 nm, revealing that the POPC-POPE bilayer adheres only weakly to the mica surface (such total squeeze-out does not occur for the L5, L8 mixtures). On adding 2 mM calcium, the most striking change is that the normalized load $(F_n(D)/R)$ that induces hemifusion increases more than 6-fold, from 80.4 ± 46.2 to 529.5 ± 207.0 mN/m, corresponding to pressures of ca. 2 to 3 MPa, comparable with those in synovial joints (see later).

The shear-force versus normal-force profiles (F_s vs. F_n, Fig. 3*B*) and the shear force versus separation distance (F_s vs. *D*) profiles inset to Fig. 3*B* show a strong increase in friction on hemifusion. Following total expulsion of the lipid, the two surfaces become rigidly coupled over the range of lateral motion applied to the top surface (so that sliding friction cannot be measured). This is expected, as the slip plane reverts from the highly lubricated one between hydrated headgroups to a much more dissipative one between acyl tails following hemifusion.

L5 mixture: DPPC-POPC-DOPC-POPE-egg SM (molar ratio 1:1:1:1:1), Fig. 3C and ***D.*** The AFM scans (Fig. 1*D*) together with the separation distance when two surfaces were in contact (Fig. 3*C*) indicate that vesicles of the five-component mixture form flat bilayers with phase-separated domains (dimensions of order 10 to 100 nanometers) distributed irregularly on the bilayer. These are likely composed of the saturated lipids in L5: Egg SM and DPPC, as such lipids can form gel-state domains by tight alkyl chain packing and phase-separate from the majority fluid phase composed of unsaturated PC lipids, similarly to "rafts" on biological membranes (34). The hybrid POPC, with one saturated and one unsaturated tail, preferentially accumulates at the interface between the gel and liquid-crystalline phases, reducing the packing incompatibility and line tension between the two phases, further stabilizing small domains in the bilayer (35, 36). After introducing 2 mM $Ca(NO_3)_2$, larger phase-separated domains appear on the bilayer—possibly because calcium binds laterally more strongly

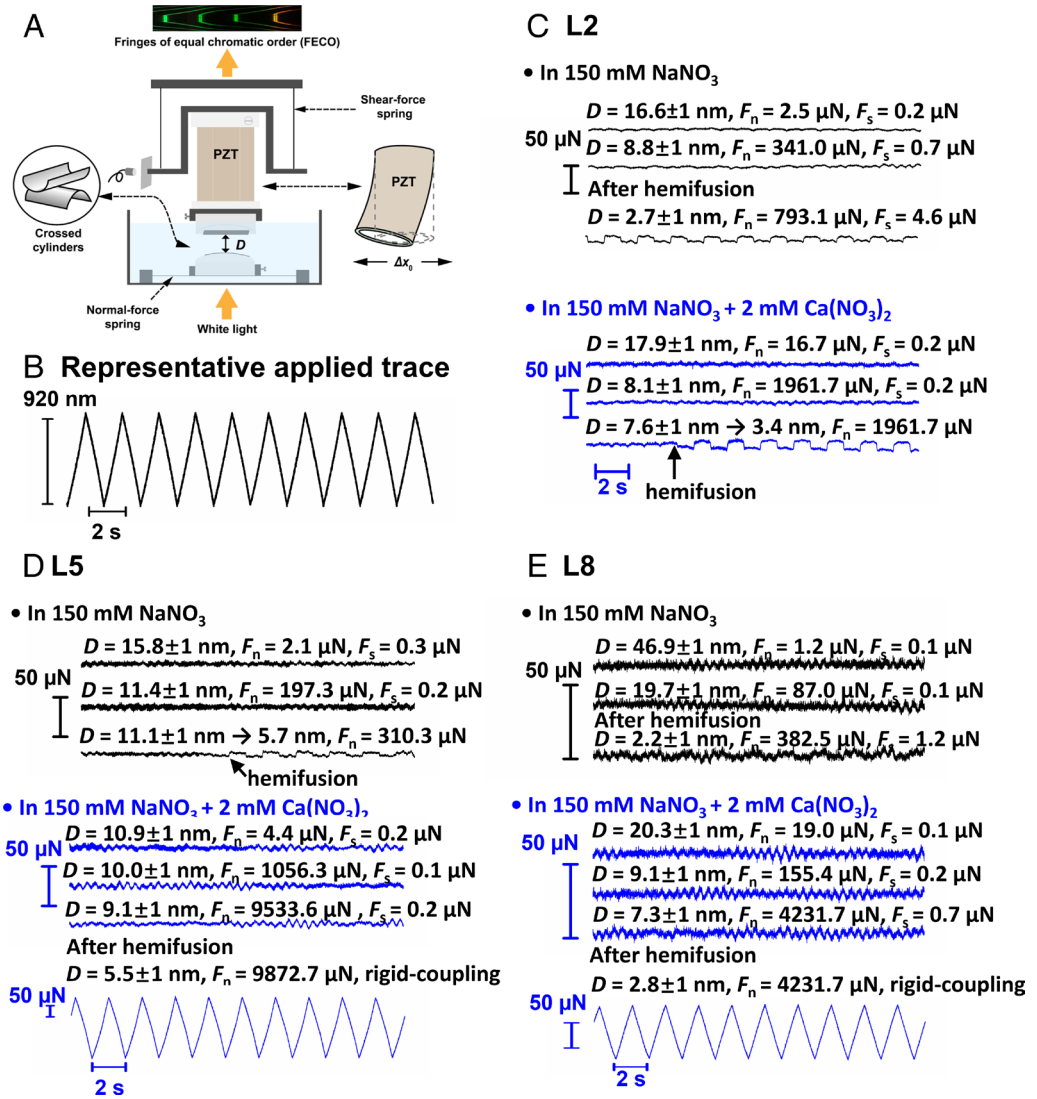

Fig. 2. Illustration of the SFB setup (*A*) and representative applied lateral motion to the upper surface (*B*), and shear force $F_s(t)$ traces (*C*–*E*) across L2, L5, and L8 dispersions, respectively. In panel (*A*), two mica surfaces are in a crossed-cylindrical configuration at a closest separation distance *D*, which is determined according to the wavelengths of fringes of equal chromatic order (FECO) using the multiple beam interference technique (the fringes shown in the *Top* panel are for two surfaces in adhesive contact). Normal and shear forces were determined by the bending of corresponding springs. Displacement of shear springs is monitored by an air-gap capacitor, as responses to the applied back-and-forth motion via the sectored PZT. In figures (*C*–*E*), black and blue traces represent those before and after adding 2 mM $Ca(NO_3)_2$. The changes in shear traces at hemifusion, indicated by an increase in F_s, were recorded for the L2 system after adding calcium (the lowest blue trace in (*C*), and for the L5 system before adding calcium (the lowest black trace in (*D*). Hemifusion was observed after applying sufficient normal force to the system and occasionally took place while recording the shear trace, as indicated by the arrows.

to Egg SM and DPPC than to POPC and DOPC (35), while the height of the patches is ca. 0.8 nm higher than the surroundings (Fig. 2*F*), attributed to the height difference between bilayers in gel and liquid-crystalline states (*SI Appendix*, Table S1). The phase-separated regions (lighter color) in Fig. 1*E* occupy ca. 13% of the area scanned.

The normal force profiles show that the bilayer thickness reaches a hard-wall at 10.4 ± 0.8 and 8.9 ± 0.8 nm, respectively, while following hemifusion, *D* decreases to 5.1 ± 1.1 and 4.6 ± 0.8 nm, respectively. Even more marked than for L2, adding calcium to the system strongly increases the critical normal load triggering hemifusion from 15.6 ± 11.6 to 831.0 ± 122.3 mN/m (Fig. 3*C*), equivalent to contact pressures of some 4 to 5 MPa.

Prior to hemifusion, the friction is extremely low (at shear-trace noise levels) with $\mu \approx 10^{-4}$ (Fig. 3*D*). Immediately following hemifusion in the absence of calcium, μ increases ca. 50-fold (to $\mu \approx 5 \times 10^{-3}$), though at the much higher loads and pressures leading to hemifusion in the presence of 2 mM calcium, we observed a rigid-coupling of two surfaces, indicating that the sliding friction exceeds the range applied shear force (F_s > 300 μN), corresponding to $\mu \gtrsim 3 \times 10^{-2}$.

L8 mixture: DPPC:POPC:DOPC:POPE:Egg SM:O-LPC:CHOL:DPPA (molar ratio 1:1:1:1:1:1:1:0.1), Fig. 3E and F. The L8 mixture consists of representatives of essentially all the major PL groups identified in synovial joints, at roughly their proportions as measured on articular cartilage surfaces (24) (*SI Appendix*, Fig. S2). It includes, in addition to the lipids in L5, also lyso-PC (O-LPC), CHOL, and a negatively charged PL (DPPA, 1.2 mol%). Lyso-PC, with a conical configuration (positive curvature), is more likely to assemble in the outer leaflet of vesicles and inhibits membrane fusion (37). CHOL is ubiquitous in PL cell membranes, and it is also found in SF (38). CHOL has an affinity to different PLs in the decreasing order SM > PC > PE, and preferentially interacts with saturated PCs over unsaturated ones; it has been shown both in experiments and in MD simulations to promote lateral segregation into phases rich in either saturated or in unsaturated lipids (39, 40). Adding CHOL

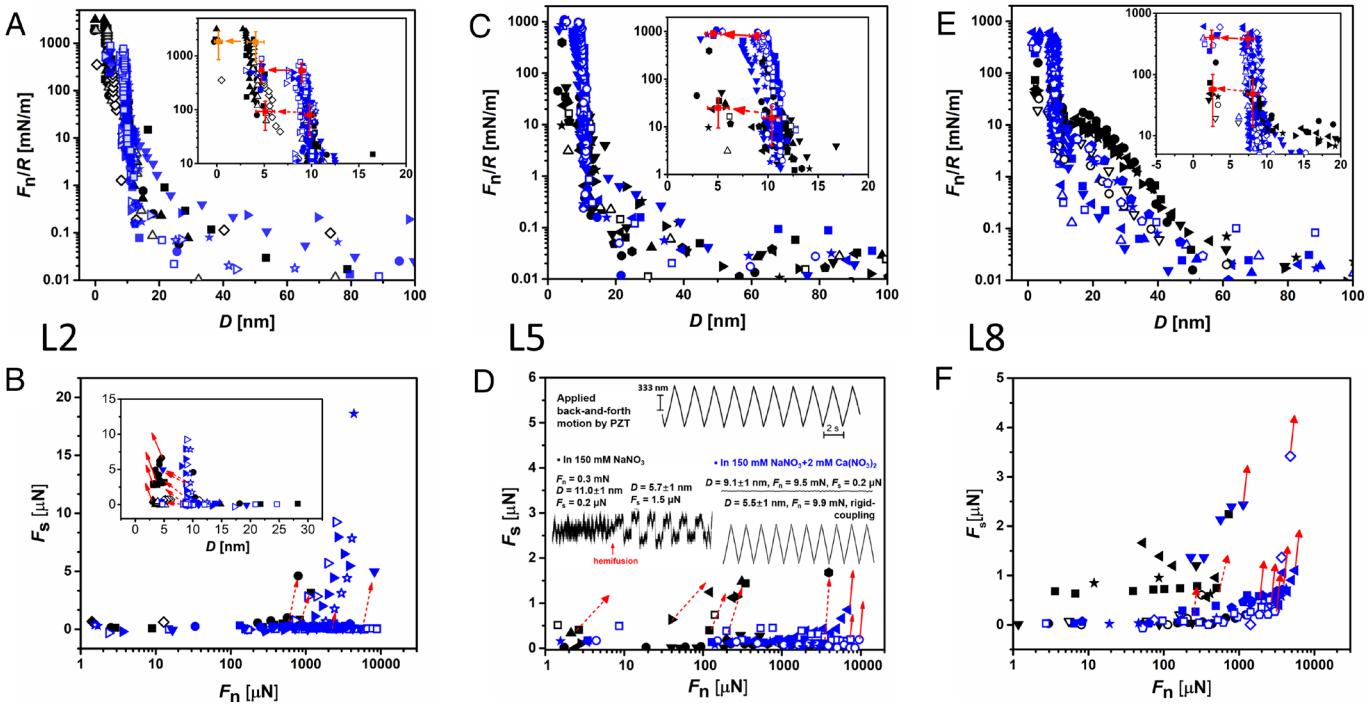

Fig. 3. Force profiles across 0.3 mM L2 (*A* and *B*), L5 (*C* and *D*), and L8 (*E* and *F*) dispersion in 150 mM $NaNO_3$ before (black symbols) and after (blue symbols) adding 2 mM $Ca(NO_3)_2$, respectively. Panels (*A*), (*C*), and (*E*): Normalized force versus separation distance (F_n/R vs. *D*) profiles. Panels (*B*), (*D*), and (*F*): Shear force versus normal force (F_s vs. F_n) profiles, *D* = 0 nm is defined as mica–mica contact in air. Solid and open symbols represent the first and subsequent approaches, respectively. Arrows in the inset of panels (*A*), (*C*), and (*E*) indicate jumps in *D* when a bilayer is removed from the contact area by hemifusion (ca. 10 to 5 nm, broken lines) or totally squeezed out (ca. 5 to 0 nm, solid line). Data for figures (*B*), (*D*), and (*F*) were extracted from shear force traces as in Fig. 2, whereas red broken arrows indicate increases in F_s observed at hemifusion in 150 mM $NaNO_3$, while the red solid arrows indicate "rigid-coupling" of two surfaces at hemifusion following Ca^{++} addition, where F_s is higher than the shear-force detection limit of the device (185 μN) and rigid-coupling occurs (see text).

to single-component PCs promotes bilayer hemifusion (19). The gel-state negatively charged PL, DPPA, not only brings negative charges to the gel-state patches but also shows particularly strong interaction with cations, particularly multivalent cations, such as Ca^{++} (41). We emphasize however, as considered further in the Discussion, that although all these lipid types are found in joints, it is not known whether they comprise part of the lubricating boundary layers on articulating cartilage in vivo.

DLS measurements (Table 1) show that the L8 vesicles are monodispersed and somewhat negatively charged. Adding calcium induces aggregation of liposomes, revealed by multiple peaks with larger sizes and a higher polydispersity (Table 1 and *SI Appendix*, Figs. S3 and S4), as well as a slight reduction in the zeta-potential. On adsorption to mica the liposomes rupture and form a planar layer with round phase-separated domains with diameter in the range of tens of nanometers (Fig. 2*G*). These may be attributed to the promotion by the CHOL of phase separation of saturated from the unsaturated lipids in L8 (39, 40). After adding 2 mM $Ca(NO_3)_2$, larger phase-separated gel-state patches are observed, and the height of these domains is ca. 1 to 2 nm higher than the surroundings (Fig. 2 *H* and *I*). This may arise from calcium binding strongly to adjacent anionic PLs, thus promoting a tighter packing of alkyl chain in the membrane and a thicker hydrophobic region (42).

The normal force profiles in Fig. 3*E* show that as for L2 and L5, hemifusion of the compressed L8 bilayers is strongly suppressed and moved to higher pressures by the presence of calcium. Thus, hemifusion is observed at critical normal loads 48.5 ± 34.6 (in the range of 19.1 to 157.1) mN/m and 384.8 ± 111.5 (in the range of 241.3 to 610.1) mN/m before and after adding 2 mM calcium salt, while *D* decreases from 8.1 ± 0.8 and 7.0 ± 1.1 nm to 2.6 ± 0.5 and 3.1 ± 0.4 nm, respectively.

The measured friction behavior (Fig. 3*F*) is similar to the other mixtures, with friction increasing strongly upon hemifusion so that the two surfaces become rigidly coupled on lateral motion of the top one (corresponding in this case to $\mu \geq$ ca. 0.07), though most of the critical loads (and thus contact pressures, see below) at hemifusion are lower than for L2 and L5.

MD Calculations. As seen above, hemifusion is the crucial step limiting efficient lubrication. To better understand how hemifusion in the different lipid mixtures occurs, an integral part of this study comprised MD calculations of the likelihood of stalk formation between the opposing bilayers, stalks being the precursors of hemifusion, as described in the *Discussion* section below.

Discussion

The main findings of this work are as follows: At low loads (low contact pressures), all three synovial lipid mixtures display excellent boundary lubrication properties ($\mu \approx 10^{-4}$ or lower). As the normal loads (and thus the contact pressures) increase beyond some critical value, the layers undergo hemifusion, at which point the friction rises abruptly. Addition of Ca^{++} to physiological concentrations (2 mM) greatly increases the magnitude of these critical loads, so that hemifusion occurs at higher contact pressures, comparable with those at articular cartilage in synovial joints during free walking (around 5 MPa) (43).

A closer examination however reveals, remarkably, that using the 5-component lipid mixture L5 leads to a lubricating layer which is more robust to hemifusion under loading and shear than either the 2-component L2 or the 8-component L8 mixtures, in the sense of sustaining very significantly higher pressures before hemifusion and a sharp rise in the friction occur. This result, shown in Fig. 4 and considered further below, indicates lubrication synergy in

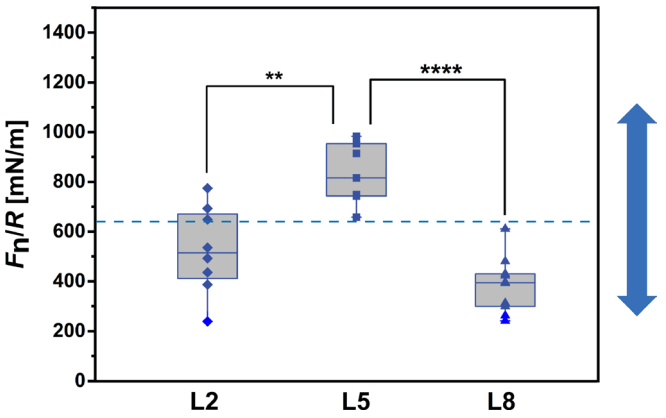

Fig. 4. Normalized forces at the critical loads for hemifusion in the presence of physiological-level calcium for the three systems. Data are presented as box plots, whereas each box shows the interquartile range and the line inside represents the median. $^{**}P \le 0.01$, $^{****}P \le 0.0001$. The blue double-arrow shows the corresponding range of maximal contact pressures at the articular cartilage surface directly measured with pressure transducers in the human hip joint during free walking (43), while the broken blue line is its mean value. Statistical analysis (unpaired *t* test) was performed using GraphPad Prism. The data were also analyzed with a one-way ANOVA with post hoc Tukey Honest Significant Difference, showing similarly significant differences between L5 and L2 and L5 and L8 (*SI Appendix*, Table S3).

suitable mixtures of lipids. It is both unexpected and strongly suggestive, shedding light on the possible origin of the proliferation of lipid types in joints from the viewpoint of cartilage lubrication. It is instructive first to consider the effect of the presence of calcium on the interactions between the lipid-coated surfaces.

Effect of Calcium. In the context of lubrication, one might have expected that the cationic Ca^{++} ions would bridge the opposing lipid layers through adhesive dipole–charge or charge–charge interactions. Indeed, the aggregation induced by Ca^{++} ions for vesicles of the L8 mixture (Table 1) indicates that such bridging occurs between the negatively charged DPPA headgroups. Adhesive bridging might be expected to increase frictional dissipation as the surfaces slide, due to hysteretic bond breakage and reformation. In contrast to this, our results reveal the opposite, counterintuitive effect: that adding physiological-level concentrations of calcium actually improves the lubrication, for all three mixtures studied, by suppressing the hemifusion of opposing bilayers, and hence the increase in friction, up to much higher loads than is the case in the absence of such ions.

We may attribute this suppression of hemifusion to the fact that the added calcium increases the intralayer cohesion by bridging adjacent zwitterionic phosphocholine, leading also to a higher areal density of the lipids (41). This increased cohesion implies that larger loads/pressures are then needed to induce hemifusion. Our findings contrast with a previous report that physiological level calcium promotes hemifusion of supported PL membranes (44). The difference arises because in the previous study, an asymmetric bilayer was used, where the lower leaflet rigidly anchored the outer, negatively charged, mixed-lipid leaflet to the substrate, and the Ca^{++} ions bridged the two bilayers strongly to induce hemifusion. This contrasts with the present study where calcium ions strengthened the much weaker bilayer/substrate interaction, while their intralayer interactions within the essentially neutral upper leaflets, enhanced by Ca^{++} as described above, rendered them more robust against hemifusion. In view of the elevated levels of Ca^{++} ions reported for OA SF relative to healthy SF higher (32, 33), it would be of interest in future work to examine the effect of different concentrations on the propensity to hemifusion.

Lipid Synergy in Articular Cartilage Lubrication. The central question that this study addresses, as posed in the Introduction, is whether the presence of many different lipid types in synovial joints could, apart from any other biological roles that they play, lead to synergy in the boundary lubrication of articular cartilage. In other words, could the presence of a particular mix of lipids in the boundary-layer coating the cartilage, composed of those lipids present in the joint, result in optimal lubrication, in the sense of lowest friction up to the highest (physiological) contact pressures? Such synergy is indeed directly indicated by our observations on lubrication by boundary layers of the L2, L5, and L8 lipid mixtures, as summarized in Fig. 4, showing the critical loads at hemifusion with boundary layers of these three different mixtures, as further detailed at the end of the *Discussion* section.

As seen clearly in Fig. 4, the boundary layers composed of the L5 mixture, comprising DPPC, POPC, DOPC, POPE, and Egg SM in equimolar concentrations, can provide low friction ($\mu \lesssim 10^{-4}$, Fig. 3*D*) prior to hemifusion up to mean critical loads that are some 50% and 100% higher than with boundary layers composed of the L2 or L8 mixtures, respectively. Thus a clear synergy arising from the multiplicity of lipids is achieved in this case. This superior lubrication ability of L5 arises by adding to the L2 mixture (POPC and POPE) the additional lipids DPPC, DOPC, and Egg SM. The mere addition of more different lipid types is not in itself the origin of the better lubrication, as seen for L8 where the components of L5 are further augmented by other lipid types found in synovial joints, but where the lubrication is very significantly inferior to that of L5 as seen in Fig. 5. Our point is not that L5 represents the actual composition of lubricating boundary layers on articular cartilage, nor even that it is the best possible combination of the lipids used in the present study (*SI Appendix*, Fig. S1 and Table S1) for forming lubricating boundary layers. Rather, the fact that a particular combination of lipids that are present in synovial joints, as in L5, provides superior lubrication—in the sense of a lubricating layer that is more robust to pressure and shear—than other combinations, is an unequivocal proof-of-concept that the proliferation of lipids in joints may indeed provide lubrication synergy. One other feature of Fig. 4 may be emphasized: The mean maximal pressure on human articular cartilage during walking, indicated by the broken line in Fig. 4, is very much in the range where lubrication breakdown due to hemifusion occurs in the mixtures used in this study. But while the mean L2 and L8 breakdown values are below this mean value, that of L5 is above it; simplistically, that suggests that a lubricating boundary layer of L5 lipids would lubricate human joints—and avoid cartilage-wear leading to OA—much more efficiently than layers of either L2 or L8.

Can we determine what an optimally lubricating lipid mixture might consist of? In principle one may measure directly the behavior of many different lipid combinations to identify the best one, but it is clearly impractical to measure more than a tiny fraction of all possible combinations of the 100+ lipids in synovial joints (thus there are close to 10^8 ways of choosing, say, a 5-lipid combination from 100 different lipids, and even a combination of 5 out of the 50 most likely lipids presents over $2*10^6$ possibilities). Alternatively, one may try to predict the lubrication properties of a lipid mixture by considering the attributes of its component lipids. For example, saturated PC lipids (such as DPPC in L5) have highly hydrated headgroups promoting low friction through the hydration lubrication mechanism (17), and are in the mechanically robust gel phase. On the other hand, they may be slow to heal once damaged (14, 21), and their bilayers are associated with a friction coefficient that is higher than that of unsaturated lipids [e.g., POPC (14)]. Such "pros" and "cons" may be considered also for other lipids

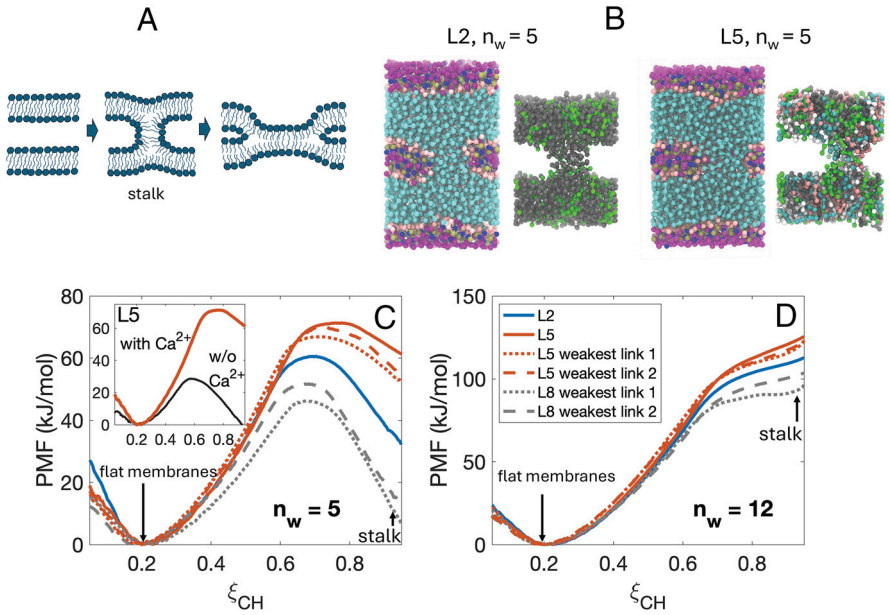

Fig. 5. MD simulations of stalk formation in lipid mixtures. (*A*) shows schematically how stalk formation leads to hemifusion and expulsion of a bilayer. (*B*) illustrates graphically the stalk formation in the L2 and L5 mixtures at hydration level n_w = 5 water molecules per lipid. L2, *Left*: magenta: water; cyan: acyl tails; gold: phosphate; blue: choline headgroup; pink: glycerol moieties. *Right* (acyl tails only): gray: POPC; green POPE. L5, *Left*: magenta: water; cyan: acyl tails; gold: phosphate; blue: choline headgroup; pink: glycerol moieties. *Right* (acyl tails only): gray: SM (egg SM); pink: POPC; green DPPC; white: DOPC; cyan: POPE. (*C*) and (*D*): The potential of mean force (PMF) plotted as a function of the reaction coordinate (extent of stalk formation), at n_w = 5 and n_w = 12 hydration levels, respectively, in presence of Ca^{++}, for the following: L2; L5 (as prepared); "weakest links" 1 & 2 for L5; and weakest links 1 & 2 for L8 (see text), color-coded as in legend in panel (*D*). For all PMF profiles, the estimated error is < 3 kJ/mol. For L5, POPC: DOPC: POPE: DPPC: DPSM, weakest-link 1 has molar ratios 1 :1 :1:1 :0.27, and weakest link 2 is 1 :1 :1 :0.6 :0.67. For L8, weakest link 1 is DOPC:CHOL in molar ratios 1:0.16, and weakest link 2 is DOPC: POPE: CHOL in ratios 1 :1 :0.3 (see text). Inset to (*C*): the effect on PMF for L5 of adding Ca^{++}.

(*SI Appendix*, Table S2). However, it is far from clear how lubrication by a mixture of lipids relates to the sum of its components; for example, phase separation and interlipid interactions may well modulate the bilayer behavior in a nonadditive manner.

Stalk Formation and Hemifusion. In view of the complexity of property-additivity and the consequent difficulty of heuristically identifying optimal combinations based just on their single-lipid properties (e.g., *SI Appendix*, Table S2), we propose a different approach to get insight into lipid mixtures that may have better boundary lubrication properties. This relies on MD to probe both frictional properties and hemifusion of compressed, sliding bilayers consisting of different lipid mixtures. Very recently we used all-atom MD to evaluate friction between two (single component) POPC lipid bilayers sliding past each other (45, 46), showing good quantitative agreement with the SFB-measured friction, and this approach can readily be extended also to friction between bilayers consisting of lipid mixtures as in the present study.

For probing the likelihood of *hemifusion* of bilayers, as seen in Fig. 3 for the mixtures used in this study, which is the limiting factor for their efficient lubrication, a different MD approach may be used. A well-known indicator of impending hemifusion is the formation of a stalk structure between interacting membranes (i.e., lipid bilayers) (47–49), as schematically shown in Fig. 5*A* below. The development of such a stalk may be monitored graphically, and its likelihood may be gauged by evaluating the potential of mean force (PMF), ΔG_{PMF}, at different values of the reaction coordinate ξ_{CH} corresponding to different stages of the stalk formation (47). Higher values of ΔG_{PMF} correspond to a lower likelihood of stalk formation and therefore of hemifusion. A molecular-level examination—via MD PMF calculations—of the factors influencing stalk formation has been provided in ref. 47.

As proof of concept that this may yield insight into the lubrication-robustness (i.e., resistance to hemifusion) of lipid mixture bilayers, we carried out such MD calculations of ΔG_{PMF} for the lipid mixtures used in this study (L2, L5, and L8), using the same MD protocols as in ref. 47, with hydration levels n_w = 5 or 12 water molecules/lipid (*SI Appendix* for detailed method). These, respectively, represent the critical hydration level for hemifusion and the full hydration level for unperturbed bilayers (47). For comparison with experiment, we use the lower bound (n_w = 5 water molecules/lipid), since hemifusion occurs under strong compression in the SFB, where the number of water molecules/headgroup reduces locally due to pressurized deformation across the contact area. In the case of the L5 mixture, we calculate ΔG_{PMF} for the as-prepared composition, but we note that the AFM micrograph (Fig. 1*E*) indicates some phase separation of the gel-phase lipids, as noted earlier. Since the majority liquid-phase regions of L5 are more prone to hemifusion, we calculate ΔG_{PMF} also for these. Estimating for L5 the extent of phase separation from Fig. 1*E* as 13% (of the total of 40% gel phase lipids DPPC and Egg SM), we examine stalk formation between a mixture of the majority liquid-phase lipids together with the residual 27% of DPPC and Egg SM, for two limiting cases (Fig. 5*C* and *D*). Stalk formation is more likely between such liquid-phase-lipids enriched mixtures, and since hemifusion initiated at such domains would lead to hemifusion of the entire bilayer, they constitute (and are designated in Fig. 5) as the weak link for stalk formation and hemifusion. For the case of the L8 mixture, the situation is more complicated, since that mixture contains CHOL which is known to cause phase separation in bilayers of mixtures of saturated and unsaturated lipids (39, 40), implying—for L8—phase-separated domains of POPC and DOPC (enriched in CHOL). Interacting bilayers of CHOL-rich DOPC have earlier been shown to have lower ΔG_{PMF} values for stalk formation than the CHOL-free DOPC bilayers (47), and as for the L5 domains above, they would constitute the weak link for stalk formation and hemifusion for L8. We therefore also examine stalk formation between DOPC/CHOL and between DOPC/POPE/CHOL layers.

The results on the likelihood of stalk formation for the three lipid mixtures (including the weak-links for L5 and L8) are presented in Fig. 5*C* and *D*.

Fig. 5*D* shows that the magnitude of ΔG_{PMF} for the as-prepared L5 mixture is higher than for the L2 mixture and remains significantly higher even when phase-separation, as indicated in Fig. 1*E*, is taken into account as noted above (weakest-link domains), i.e., this result predicts clearly that L5 would better resist hemifusion than L2. A simple Arrhenius transition state model (*SI Appendix*), based on the differences in PMF maxima shown in Fig. 5*C*, suggests that the rate of stalk formation for the L5 mixture is at least an order of magnitude lower than for the L2 mixture, emphasizing the effects of synergy. Likewise, for CHOL-induced phase-separated regions in L8, the magnitude of ΔG_{PMF} is significantly lower than for L2, predicting more likely stalk formation, and thus hemifusion, for the 8-component mixture relative to the 2-component one. This ranking of hemifusion likelihood holds for both $n_w = 5$ and $n_w = 12$ cases, though it is more marked in the former where stalk formation is an energetically favored state. These predictions of the MD calculations, i.e., that the likelihood of hemifusion decreases as L8 > L2 > L5, so that the critical pressure to induce hemifusion increases as L8 < L2 < L5, are exactly what is seen in the experimental SFB results, Fig. 4. This behavior could not have been predicted a priori based simply on mixing of the qualitative properties of the single lipid bilayers (e.g., *SI Appendix*, Table S2). This proof-of-concept demonstration thus strongly supports the notion that MD may be a powerful tool in gaining insight into nature's multilipid synergy in boundary lubrication of cartilage. We have also examined the effect on the PMF of adding Ca^{++} to the lipid mixtures, as in the inset to Fig. 5*D*: The presence of Ca^{++} leads to a very marked increase in the PMF, i.e., stalk formation and thus hemifusion is suppressed, precisely as seen in the SFB experiments. This effect too could not have been predicted a priori by heuristic considerations, indeed it is somewhat counterintuitive as earlier discussed. It is finally of interest that stalk formation as a precursor to hemifusion has to date been considered mostly in the biochemical context of cell membrane interactions or of vesicle-cell fusion; here, it plays a central role in lipid-mediated lubrication, with relevance to cartilage lubrication and its connection to joint homeostasis. It is also appropriate to recall several aspects of our study that are relevant to such lubrication: the use in our mixtures of some of the most common lipids found in joints; the salt concentrations used, including divalent salt, that are comparable to those in SF; and measurements up to local contact pressures spanning those between cartilage in joints.

To summarize, the lubrication synergy as shown in the present study arises because bilayers formed exclusively of lipids in their liquid phase (as opposed to gel phase) provide better lubrication (as they are more highly hydrated and form smooth bilayers) and faster healing following damage (as the lipids are more fluid), but are at the same time more prone to hemifusion (when compressed against similar bilayers), which destroys the good lubrication. This has been directly shown in earlier studies (14). Meanwhile, bilayers formed exclusively of lipids in the gel phase provide less good lubrication (their headgroups are less hydrated, and they do not readily form smooth bilayers but remain in the less-smooth, thus higher-friction, vesicular phase where liposomes remain intact on the substrate) and also heal less readily, as the lipids are much less mobile; but they are more resistant to hemifusion (14). By suitably combining liquid-phase and gel-phase lipids (and possibly others in the synovial joint), it is therefore possible to achieve layers that are at the same time good lubricants, heal rapidly following any damage, and, especially, better resist hemifusion, attributes which, taken together, are superior—from the point of view of desirable lubricant properties—to those of the individual components on their own. This is further detailed with regard to our particular mixtures in *SI Appendix*.

Conclusions

We have shown that mixtures of lipids present in synovial joints may form boundary layers that possess excellent lubrication properties—comparable with those of healthy joints up to physiological pressures—while at the same time, they may combine desirable features of their different components. By revealing that particular combinations of these lipids (e.g., L5) can be significantly superior as lubricating layers compared to other combinations with either more (L8) or fewer (L2) lipid components, we unambiguously demonstrate the possibility of multilipid synergy. While we do not claim to have identified the optimal composition of such a layer, it is nonetheless clear from our results on a limited sample of synovial joint lipids that such an optimal composition is possible. This may advance our understanding of the proliferation of different lipid types in healthy synovial joints: Purely from a lubrication point of view, essential for joint homeostasis, such a proliferation, enabling optimal lubrication, is clearly beneficial. Importantly, we were able to show, in a proof-of-concept demonstration, that MD simulations are able to predict accurately the relative robustness against hemifusion of the different lipid mixtures (specifically, that L5 is less likely to hemifuse than L2, which in turn is less likely to hemifuse than L8, which indeed were key observations). The synergy we demonstrate may also help in identifying molecular design principles for better lubricating lipid mixtures. For example, the idea that lipid bilayer domains where a small fraction of saturated lipids is mixed into a liquid-phase majority component to suppress hemifusion; or the awareness that certain lipids (e.g., CHOL) may lead to unfavorable phase separation in certain circumstances and need to be considered with care. In the light of recent suggestions (2) that intra-articularly (IA) injected liposomes may serve to augment or repair the body's natural biolubrication mechanisms at the articular cartilage surface, our results may also point how to identify and implement optimal liposome compositions for such IA administration.

Materials and Methods

Materials. Eight different lipids as detailed below representing the main types in human synovial joints were used in this study: Egg SM (Egg SM, whose fatty acids distribution is 86% 16:0, 6% 18:0, 3% 22:0, 3% 24:1, and 2% unknown) and 1-oleoyl-2-hydroxy-*sn*-glycero-3-phosphocholine (O-LPC, purity > 99% LPC, may contain up to 10% of the 2-LPC isomer), and 1-palmitoyl-2-oleoyl-glycero-3-phosphoethanolamine (POPE) were purchased from Avanti Polar Lipids, Inc. (Alabama, USA). DPPC, POPC, 1,2-dioleoyl-*sn*-glycero-3-phosphocholine (DOPC), and 1,2-palmitoyl-phosphatidic acid (sodium salt) (DPPA) were obtained from Lipoid GmbH (Ludwigshafen, Germany). CHOL (≥99%), sodium nitrate ($NaNO_3$) 99.99 Suprapur®, and calcium nitrate tetrahydrate ($Ca(NO_3)_2 4H_2O$) 99.95 Suprapur® were purchased from Merck KGaA (Darmstadt, Germany). Chloroform (analytical reagent grade) and methanol (HPLC grade) were purchased from Bio-Lab Ltd. (Jerusalem, Israel). Conductivity water (resistivity 18.20 MΩ·cm, total organic carbon content ≤2 ppb) was obtained with a Thermo Scientific™ Barnstead™ water purification system. The chemical structures and physiochemical properties of these 8 lipids (POPC, POPE, DPPC, DOPC, Egg SM, O-LPC, Chol, and DPPA) are shown in *SI Appendix*, Fig. S1 and Table S1.

Preparation of SUVs. The preparation of SUVs was carried out using a hydration–extrusion method. Lipids were mixed by dissolving separately in a solvent of chloroform and methanol (2:1, v:v) except for POPE, which was dissolved in chloroform. After that, appropriate amounts of different PL solutions were thoroughly mixed in a glass vial. Organic solvents were then removed by purging nitrogen gas for at least one day and followed by lyophilization overnight. The SUVs were prepared by a thin-film hydration followed by the extrusion method.

The procedures were similar to those described previously (21) except for a few modifications: A 150 mM $NaNO_3$ aqueous solution was used as dispersant, and temperature was controlled at ca. 10 °C higher than the highest phase transition temperature of individual PL components for both sonication bath and extruder jacket. The prepared SUV dispersions were cooled down to room temperature and kept at 4 °C before use.

Size Distribution, Polydispersity Index (PDI), and Zeta Potential. The prepared SUVs were measured on a Malvern Zetasizer Nano ZS instrument. Size analysis were performed with a backscattering angle at 173°, and the values were determined according to the Stokes–Einstein equation. Liposomes with a total lipid concentration of 0.3 mM prepared in 150 mM $NaNO_3$ or after adding 2 mM $Ca(NO_3)_2$ were directly used for size distribution measurements and were diluted by ten-fold with water for zeta potential measurements.

AFM. The AFM was used to probe the morphology of SUVs on mica. An Asylum MPF-3D atomic force microscope and Bruker's SNL-10 probes were used. All the scans were performed under aqueous environment in tapping mode. Samples were prepared by introducing 0.3 mM SUVs in 150 mM $NaNO_3$ or in 150 mM $NaNO_3$ with 2 mM $Ca(NO_3)_2$ to a petri dish with a freshly cleaved mica facet glued on the bottom. After incubating for more than 4 h, scans were performed under the same aqueous solution.

SFB. The normal (F_n) and shear forces (F_s) were measured at different surface separations (D) between two back-silvered mica surfaces in a crossed-cylinder configuration with an SFB. A schematic of the SFB setup is shown in Fig. 2*A*. Its details and the experimental procedures have been elaborated previously (50). Briefly, the wavelengths of multiple-beam interference FECO transmitted between the surfaces were monitored to determine D; F_n was calculated according to the relative difference between the displacement of the normal spring (spring constant k_n) and the applied displacement; and F_s was calculated by applying fast Fourier transform to the recorded lateral displacement of the shear spring (spring constant k_s), which were monitored by an air-gap capacitor as responses to the lateral back-and-forth movements applied to the upper lens through the piezoelectric tube (PZT). The friction coefficient μ was calculated by the ratio of shear force F_s required to slide the surfaces and the corresponding normal load F_n compressing them, that is, $\mu = F_s/F_n$.

Before adding calcium, the two surfaces were nonadhesive, and it was difficult to measure the flattening of the fringes. Thus, normal pressure at hemifusion P_{hemi} was estimated via the Hertzian model, $P_{hemi} = F_{n,hemi}/(\pi(F_{n,hemi}R/K)^{2/3})$, where $K = 5 \times 10^{-9}$ N/m^2 was adopted as the effective elastic modulus of the mica/glue combination (17). After adding calcium, the normal pressure P_{hemi} applied to the contact area at hemifusion was calculated directly by the measurement of normal force $F_{n,hemi}$ and measured fringe flattening radius a at hemifusion, $P_{hemi} = F_{n,hemi}/A = F_{n,hemi}/(\pi a^2)$. We note that while the magnitude of $F_{n,hemi}$ is accurately known from the extent of measured spring-bending, the contact area a is less accurately measured from the fringe-tip flattening, particularly when it is not large, so that a difference in P values of up to ± 30% or sometimes more under the same conditions may be obtained by these two methods (17).

At the beginning of the measurements, mica–mica contact in air corresponding to $D = 0$ nm was measured. After that, the boat was filled with 150 mM $NaNO_3$ solution to which was then added 0.8 mL of 6 mM mixed PLs-SUV dispersion prepared in the same salt solution to reach a final lipid concentration at ca. 0.3 mM, in the range of values reported in healthy SF (26).

Measurements were carried out after incubating for more than four hours to reach an equilibrium. After force profile measurements, $Ca(NO_3)_2$ aqueous solution was introduced to the boat, reaching a final concentration of 2 mM, which is in the mid-range of those identified in human SF (32), and force profiles were measured again. All the data presented below were collected from at least two independent experiments and several contact points in each experiment.

MD Simulations of the PMF Calculation of the Stalk Formation. The PMF calculation was performed with the protocol described in ref. 47 and carried out with the modified GROMACS version published by ref. 47 in the GitHub repository. It implemented a stalk formation reaction coordinate ξ_{CH} which describes the hydrophobic connectivity between the two bilayer membranes and allows a stalk to form artificially by applying a harmonic restraint along the reaction coordinate. To acquire a single PMF, multiple steps of GROMACS simulations, manipulation of structure files, and indexing of groups within the structure were carried out, which were all automized using in-house Bash scripts. The steps are briefly described below.

The structures of the single bilayers were generated from the CHARMM–GUI interface using the Martini coarse-grained force field version 2.2 (51–53). Each single membrane contained 64 lipids/monolayer, sufficient to exclude the size effect for the L2 and L5 mixtures which are free of CHOL. For the CHOL-containing L8 mixture, the energy barrier to stalk formation ΔG_{PMF} may be overestimated but does not change our conclusion that the weakest links of the L8 mixture are the least resistive to hemifusion in all systems tested (see main text) (47). 0.5 mol $CaCl^2$/mol lipid was added to the system with parameters taken from the Martini 2.0 force field. Ca^{2+} and Cl^- ions are represented as Lennard–Jones particles with parameters calibrated inclusive of the hydration shell. Note that due to the limitation of the Martini description of divalent ions, the results are not to be considered quantitatively, but only for our goal of ranking the likelihood of stalk formation. The energy of the single membrane was then minimized. Excess water was then removed from the system such that the hydration level of the outer leaflet is 36 water molecules/lipid, and the hydration level of the inner leaflet is 5 or 12 water molecules/lipid. The single membrane was then replicated, flipped vertically, translated, and stacked to obtain a symmetric double-bilayer system. By assuming a hydration shell of 7 and 12 water molecules/Ca^{2+}, respectively, for the dehydrated and fully hydrated cases based on NMR studies (54), we estimated that the Ca^{2+} concentration in the inner compartment of the systems of the two hydration levels $n_w = 5$ and $n_w = 12$ are, respectively, 1.3 M and 2.2 M. This is consistent with previous second harmonic microscopy observations, that the ion concentration in the lipid headgroup region is 1 to 3 M (55, 56).

The double-bilayer system then undergoes energy minimization and equilibration for 25 ns until the box dimensions and energy are stabilized. The equilibrated system was processed following the exact steps and GROMACS parameters and restraints published in ref. 47. First, the carbon tails of the systems were pulled using the harmonic potential (k = 3,000 kJ/mol) into the inner intermembrane space to artificially induce the stalk structure within 200 ns. For the umbrella sampling, 19 initial structures were extracted from the trajectories evenly along the reaction coordinate ξ_{CH}. PMFs were calculated using umbrella sampling with these initial frames using the same harmonic restraints at the corresponding ξ_{CH} values, with each run persisting 200 ns at a time step of 18 fs. The PMFs were then calculated using the gmx wham function of GROMACS 2023.2. The error is estimated following the method proposed in ref. 47, where separated PMFs were generated using pieces of the umbrella sampling simulations, respectively, at 50 to 100 ns, 100 to 150 ns, and 150 to 200 ns intervals. The error is estimated as the SD between these PMF curves. The average error along a given PMF curve is 1.0 to 1.6 KJ/mol while the maximum error is 2.1 to 3.3 KJ/mol.

Data, Materials, and Software Availability. All study data are included in the article and/or *SI Appendix*.

ACKNOWLEDGMENTS. We thank the European Research Council (Advanced Grant CartiLube 743016 and Proof of Concept Grant BiofilmEradicate 101069414), the McCutchen Foundation, the Israel Science Foundation–National Natural Science Foundation of China joint research program (Grant 3618/21), the Israel Ministry of Science and Technology (Grant 3-15716), and the Israel Science Foundation (Grant 1229/20) for financial support. This work was made possible partly through the historic generosity of the Perlman family.

Author affiliations: [a]Department of Molecular Chemistry and Materials Science, Weizmann Institute of Science, Rehovot 76100, Israel

1. J. Finkelstein, M. T. Heemels, S. Shadan, U. Weiss, Lipids in health and disease. *Nature* **510**, 47–47 (2014), 10.1038/510047a.
2. W. Lin, J. Klein, Recent progress in cartilage lubrication. *Adv. Mater.* **33**, 2005513 (2021), 10.1002/adma.202005513.
3. W. Lin *et al.*, Cartilage-inspired, lipid-based boundary-lubricated hydrogels. *Science* **370**, 335–338 (2020).
4. S. Jahn, J. Seror, J. Klein, Lubrication of articular cartilage. *Annu. Rev. Biomed. Eng.* **18**, 235–258 (2016), 10.1146/annurev-bioeng-081514-123305.

5. J. Seror, L. Zhu, R. Goldberg, A. J. Day, J. Klein, Supramolecular synergy in the boundary lubrication of synovial joints. *Nat. Comm.* **6**, 6497 (2015), 10.1038/ncomms7497.
6. F. Dell'accio, T. L. Vincent, Joint surface defects: Clinical course and cellular response in spontaneous and experimental lesions. *European. Cells Mater.* **20**, 210–217, (2010).
7. Hilšer *et al.*, A new insight into more effective viscosupplementation based on the synergy of hyaluronic acid and phospholipids for cartilage friction reduction. *Biotribology* **25**, 100166 (2021), 10.1016/j.biotri.2021.100166.
8. T. Murakami, S. Yarimitsu, K. Nakashima, Y. Sawae, N. Sakai, Influence of synovia constituents on tribological behaviors of articular cartilage. *Friction* **1**, 150–162 (2013), 10.1007/s40544-013-0010-6.
9. G. A. Ateshian, The role of interstitial fluid pressurization in articular cartilage lubrication. *J. Biomechanics* **42**, 1163–1176 (2009), 10.1016/j.jbiomech.2009.04.040.
10. T. A. Schmidt, N. S. Gastelum, Q. T. Nguyen, B. L. Schumacher, R. L. Sah, Boundary lubrication of articular cartilage - Role of synovial fluid constituents. *Arthritis Rheum.* **56**, 882–891 (2007).
11. Goldberg *et al.*, Boundary lubricants with exceptionally low friction coefficients based on 2D close-packed phosphatidylcholine liposomes. *Adv. Mat.* **23**, 3517–3521 (2011).
12. W. F. Lin *et al.*, Lipid–hyaluronan synergy strongly reduces intrasynovial tissue boundary friction. *Acta Biomaterialia* **83**, 314–321 (2019), 10.1016/j.actbio.2018.11.015.
13. Y. Duan, Y. Liu, J. Li, S. Feng, S. Wen, AFM study on superlubricity between Ti6Al4V/polymer surfaces achieved with liposomes. *Biomacromolecules* **20**, 1522–1529 (2019), 10.1021/acs.biomac.8b01683.
14. R. Sorkin, N. Kampf, L. Zhu, J. Klein, Hydration lubrication and shear-induced self-healing of lipid bilayer boundary lubricants in phosphatidylcholine dispersions. *Soft Matter* **12**, 2773–2784 (2016), 10.1039/C5SM02475G.
15. Y. Cao, N. Kampf, W. Lin, J. Klein, Normal and shear forces between boundary sphingomyelin layers under aqueous conditions. *Soft Matter* **16**, 3973–3980 (2020), 10.1039/D0SM00215A.
16. H. BriscoeW *et al.*, Boundary lubrication under water. *Nature* **444**, 191–194 (2006).
17. R. Sorkin, N. Kampf, Y. Dror, E. Shimoni, J. Klein, Origins of extreme boundary lubrication by phosphatidylcholine liposomes. *Biomaterials* **34**, 5465–5475 (2013).
18. L. Yang, X. Zhao, Z. Ma, S. Ma, F. Zhou, An overview of functional biolubricants. *Friction* **11**, 23–47 (2023), 10.1007/s40544-022-0607-8.
19. R. Sorkin, N. Kampf, J. Klein, Effect of cholesterol on the stability and lubrication efficiency of phosphatidylcholine surface layers. *Langmuir* **33**, 7459–7467 (2017), 10.1021/acs.langmuir.7b01521.
20. Y. Cao, N. Kampf, M. K. Kosinska, J. Steinmeyer, J. Klein, Interactions between bilayers of phospholipids extracted from human osteoarthritic synovial fluid. *Biotribology* **25**, 100157 (2021), 10.1016/j.biotri.2020.100157.
21. Y. Cao, N. Kampf, J. Klein, Boundary Lubrication, hemifusion, and self-healing of binary saturated and monounsaturated phosphatidylcholine mixtures. *Langmuir* **35**, 15459–15468 (2019), 10.1021/acs.langmuir.9b01660.
22. B. A. Hills, B. D. Butler, Surfacants identified in synovial fluid and their ability to act as boundary lubricants. *Ann. Rheum. Dis.* **43**, 641–648 (1984).
23. V. Saikko, T. Ahlroos, Phospholipids as boundary lubricants in wear tests of prosthetic joint materials. *Wear* **207**, 86–91 (1997), 10.1016/S0043-1648(96)07482-0.
24. A. V. Sarma, G. L. Powell, M. LaBerge, Phospholipid composition of articular cartilage boundary lubricant. *J. Orthopaedic Res.* **19**, 671–676 (2001).
25. C. I. Matei *et al.*, Ultrastructural analysis of healthy synovial fluids in three mammalian species. *Microsc. Microanal.* **20**, 903–911 (2014), 10.1017/S1431927614000415.
26. M. K. Kosinska *et al.*, A lipidomic study of phospholipid classes and species in human synovial fluid. *Arthritis Rheum.* **65**, 2323–2333 (2013).
27. M. K. Kosinska *et al.*, Sphingolipids in human synovial fluid - A lipidomic study. *PLOS ONE* **9**, e91769 (2014), 10.1371/journal.pone.0091769.
28. B. A. Hills, Oligolamellar lubrication of joints by surface active phospholipid. *J. Rheumatol.* **16**, 82–91 (1989).
29. B. A. Hills, Boundary lubrication in vivo. *Proc. Inst. Mech. Eng. H* **214**, 83–94 (2000).
30. A.-M. Mustonen *et al.*, Distinct fatty acid signatures in infrapatellar fat pad and synovial fluid of patients with osteoarthritis versus rheumatoid arthritis. *Arthritis Res. Ther.* **21**, 124 (2019), 10.1186/s13075-019-1914-y.
31. C. L. Wu, K. A. Kimmerling, D. Little, F. Guilak, Serum and synovial fluid lipidomic profiles predict obesity-associated osteoarthritis, synovitis, and wound repair. *Sci. Rep.* **7**, 44315 (2017), 10.1038/srep44315.
32. B. Madea, C. Kreuser, S. Banaschak, Postmortem biochemical examination of synovial fluid–a preliminary study. *Forensic. Sci. Int.* **118**, 29–35 (2001), 10.1016/s0379-0738(00)00372-8.
33. A. Yavorskyy, A. Hernandez-Santana, B. Shortt, G. McCarthy, G. McMahon, Determination of calcium in synovial fluid samples as an aid to diagnosing osteoarthritis. *Bioanalysis* **2**, 189–195 (2010), 10.4155/bio.09.163.
34. D. Lingwood, K. Simons, Lipid rafts as a membrane-organizing principle. *Science* **327**, 46–50 (2010), 10.1126/science.1174621.
35. O. Szekely, Y. Schilt, A. Steiner, U. Raviv, Regulating the size and stabilization of lipid raft-like domains and using calcium ions as their probe. *Langmuir* **27**, 14767–14775 (2011), 10.1021/la203074q.
36. B. Palmieri, S. A. Safran, Hybrid lipids increase the probability of fluctuating nanodomains in mixed membranes. *Langmuir* **29**, 5246–5261 (2013), 10.1021/la4006168.
37. P. L. Yeagle, F. T. Smith, J. E. Young, T. D. Flanagan, Inhibition of membrane fusion by lysophosphatidylcholine. *Biochemistry* **33**, 1820–1827 (1994), 10.1021/bi00173a027.
38. G. G. Bole, Synovial fluid lipids in normal individuals and patients with rheumatoid arthritis. *Arthritis Rheum.* **5**, 589–601 (1962), 10.1002/art.1780050606.
39. O. Engberg *et al.*, The affinity of cholesterol for different phospholipids affects lateral segregation in bilayers. *Biophys. J.* **111**, 546–556 (2016), 10.1016/j.bpj.2016.06.036.
40. G. A. Pantelopulos, J. E. Straub, Regimes of complex lipid bilayer phases induced by cholesterol concentration in MD simulation. *Biophys. J.* **115**, 2167–2178 (2018), 10.1016/j.bpj.2018.10.011.
41. U. R. Pedersen, C. Leidy, P. Westh, G. H. Peters, The effect of calcium on the properties of charged phospholipid bilayers. *Biochim. Biophys. Acta* **1758**, 573–582 (2006), 10.1016/j.bbamem.2006.03.035.
42. A. Alessandrini, P. Facci, Phase transitions in supported lipid bilayers studied by AFM. *Soft Matter* **10**, 7145–7164 (2014), 10.1039/C4SM01104J.
43. K. C. Morrell, W. A. Hodge, D. E. Krebs, R. W. Mann, Corroboration of in vivo cartilage pressures with implications for synovial joint tribology and osteoarthritis causation. *Proc. Natl. Acad. Sci. U.S.A.* **102**, 14819–14824 (2005), 10.1073/pnas.0507117102.
44. X. Banquy, K. Kristiansen, D. W. Lee, J. N. Israelachvili, Adhesion and hemifusion of cytoplasmic myelin lipid membranes are highly dependent on the lipid composition. *Biochim. Biophys. Acta* **1818**, 402–410 (2012), 10.1016/j.bbamem.2011.10.015.
45. D. Jin, J. Klein, Tuning interfacial energy dissipation via topologically electro-convoluted lipid-membrane boundary layers. arXiv [Preprint] (2023). https://arxiv.org/abs/2303.08555 (Accessed 25 September 2024).
46. Y. Zhang, D. Jin, R. Tivony, N. Kampf, J. Klein, Cell-inspired, massive electromodulation of friction via transmembrane fields across lipid bilayers. *Nat. Mater.* (2024), 10.1038/s41563-024-01926-9.
47. C. S. Poojari, K. C. Scherer, J. S. Hub, Free energies of membrane stalk formation from a lipidomics perspective. *Nat. Commun.* **12**, 6594 (2021), 10.1038/s41467-021-26924-2.
48. Y. G. Smirnova, S.-J. Marrink, R. Lipowsky, V. Knecht, Solvent-exposed tails as prestalk transition states for membrane fusion at low hydration. *J. Am. Chem. Soc.* **132**, 6710–6718 (2010), 10.1021/ja910050x.
49. L. Yang, H. W. Huang, Observation of a membrane fusion intermediate structure. *Science* **297**, 1877–1879 (2002), 10.1126/science.1074354.
50. W. Lin, J. Klein, Direct measurement of surface forces: Recent advances and insights. *Appl. Phys. Rev.* **8**, 031316 (2021), 10.1063/5.0059893.
51. P. C. Hsu *et al.*, CHARMM-GUI martini maker for modeling and simulation of complex bacterial membranes with lipopolysaccharides. *J. Comput. Chem.* **38**, 2354–2363 (2017), 10.1002/jcc.24895.
52. S. Jo, T. Kim, V. G. Iyer, W. Im, CHARMM-GUI: A web-based graphical user interface for CHARMM. *J. Comput. Chem.* **29**, 1859–1865 (2008), 10.1002/jcc.20945.
53. Y. Qi *et al.*, CHARMM-GUI martini maker for coarse-grained simulations with the martini force field. *J. Chem. Theory Comput.* **11**, 4486–4494 (2015), 10.1021/acs.jctc.5b00513.
54. A. Zhang, H. Yu, C. Liu, C. Song, The Ca(2+) permeation mechanism of the ryanodine receptor revealed by a multi-site ion model *Nat. Commun.* **11**, 922 (2020), 10.1038/s41467-020-14573-w.
55. C. Lütgebaucks, C. Macias-Romero, S. Roke, Characterization of the interface of binary mixed DOPC:DOPS liposomes in water: The impact of charge condensation. *J. Chem. Phys.* **146**, 044701 (2017), 10.1063/1.4974084.
56. D. Roesel, M. Eremchev, C. S. Poojari, J. S. Hub, S. Roke, Ion–Induced transient potential fluctuations facilitate pore formation and cation transport through lipid membranes. *J. Am. Chem. Soc.* **144**, 23352–23357 (2022), 10.1021/jacs.2c08543.